Nanoscale

PAPER

Cite this: *Nanoscale*, 2016, **8**, 19769

The structural and electronic properties of $NbSi_n^{-/0}$ (n = 3–12) clusters: anion photoelectron spectroscopy and *ab initio* calculations†

Sheng-Jie Lu,[a,b] Guo-Jin Cao,[c] Xi-Ling Xu,[a,b] Hong-Guang Xu*[a,b] and Wei-Jun Zheng*[a,b]

Received 22nd September 2016,
Accepted 8th November 2016

DOI: 10.1039/c6nr07480d

www.rsc.org/nanoscale

Niobium-doped silicon clusters, $NbSi_n^-$ (n = 3–12), were generated by laser vaporization and investigated by anion photoelectron spectroscopy. The structures and electronic properties of $NbSi_n^-$ anions and their neutral counterparts were investigated with *ab initio* calculations and compared with the experimental results. It is found that the Nb atom in $NbSi_n^{-/0}$ prefers to occupy the high coordination sites to form more Nb–Si bonds. The most stable structures of $NbSi_{3-7}^{-/0}$ are all exohedral structures with the Nb atom face-capping the Si_n frameworks. At n = 8, both the anion and neutral adopt a boat-shaped structure and the openings of the boat-shaped structures remain unclosed in $NbSi_{9-10}^{-/0}$ clusters. The most stable structure of the $NbSi_{11}^-$ anion is endohedral, while that of neutral $NbSi_{11}$ is exohedral. The global minima of both the $NbSi_{12}^-$ anion and neutral $NbSi_{12}$ are D_{6h} symmetric hexagonal prisms with the Nb atom at the center. The perfect D_{6h} symmetric hexagonal prism of $NbSi_{12}^-$ is electronically stable as it obeys the 18-electron rule and has a shell-closed electronic structure with a large HOMO–LUMO gap of 2.70 eV. The molecular orbital analysis of $NbSi_{12}^-$ suggests that the delocalized Nb–Si_{12} ligand interactions may contribute to the stability of the D_{6h} symmetric hexagonal prism. The AdNDP analysis shows that the delocalized 2c–2e Si–Si bonds and multicenter-2e $NbSi_n$ bonds are important for the structural stability of the $NbSi_{12}^-$ anion.

1. Introduction

Transition-metal (TM)-doped silicon clusters are of particular interest because the TM dopants not only can stabilize the fullerene-like cage structures of silicon clusters,[1–4] but also can induce novel physical and chemical properties such as different charge-transfer states, large highest occupied molecular orbital–lowest unoccupied molecular orbital (HOMO–LUMO) gaps, tunable magnetic properties and hyperpolarizablity.[5–10] TM-doped silicon clusters may be used as potential building blocks of silicon-based nanomaterials for production of miniaturized electronic devices.[11–15]

Niobium is widely used in the alloy industry. A Nb atom has a $4d^45s^1$ valence electron configuration, and therefore, shows an s-to-d electron promotion compared to the $3d^34s^2$ valence electron configuration of a V atom in the same group in the period table. This may lead to a unique bonding behaviour of the Nb atom when it interacts with Si atoms. Amorphous thin Nb_xSi_{1-x} films can be used to study the mechanism of superconductor–insulator transitions (SIT).[16–18] Niobium silicide films or alloys have a range of applications in digital superconducting electronics (SCE)[19] and in bolometers for astrophysical particle detection (such as detection of weakly interacting massive particles, cosmic microwaves, X-rays, or dark matter).[20–22] In addition, niobium silicides have potential applications in aircraft turbine engines owing to their good mechanical properties at both high and low temperatures.[23] Investigating the detailed structural and electronic properties of Nb-doped silicon clusters not only can provide valuable information for production of cluster-assembled materials, but is also important for understanding the microscopic mechanisms in NbSi films and metal–semiconductor alloys.

The structures of Nb-doped silicon clusters have been studied previously by a number of theoretical calculations.[24–29] The $NbSi^-$ anion was studied *via* a photoelectron imaging experiment and *ab initio* calculations,[30] and the $NbSi_n^-$ anions

[a]*Beijing National Laboratory for Molecular Sciences, State Key Laboratory of Molecular Reaction Dynamics, Institute of Chemistry, Chinese Academy of Sciences, Beijing 100190, China. E-mail: xuhong@iccas.ac.cn, zhengwj@iccas.ac.cn; Fax: +86 10 62563167; Tel: +86 10 62635054*
[b]*University of Chinese Academy of Sciences, Beijing 100049, China*
[c]*Institute of Molecular Science, Shanxi University, Taiyuan 030006, China*
†Electronic supplementary information (ESI) available. See DOI: 10.1039/c6nr07480d

in the size range of n = 6–18 were studied with anion photoelectron spectroscopy.[31] The $NbSi_n^+$ cations in the size range of n = 6–20 were studied by mass spectrometry and H_2O adsorption reactivity experiments,[32] and those in the range of n = 4–12 were investigated using argon-tagged infrared multiphoton dissociation (IR-MPD) experiments and density functional theory (DFT) calculations.[33] In this work, in order to obtain better photoelectron spectra of $NbSi_n^-$ clusters especially for the small size and to get more detailed information regarding the structural and electronic properties of the $NbSi_n$ clusters, we investigated the $NbSi_n^{-/0}$ (n = 3–12) clusters using anion photoelectron spectroscopy and *ab initio* calculations.

2. Experimental and theoretical methods

2.1 Experimental methods

The experiments were conducted using a home-built apparatus consisting of a laser vaporization cluster source, a time-of-flight mass spectrometer, and a magnetic-bottle photoelectron spectrometer, which has been described elsewhere.[34] The $NbSi_n^-$ cluster anions were generated in the laser vaporization source by laser ablation of a rotating and translating disk target (13 mm diameter, Nb : Si mole ratio 1 : 1) with the second harmonic (532 nm) light pulses from a Nd:YAG laser (Continuum Surelite II-10), while helium gas with ~0.4 MPa backing pressure was allowed to expand through a pulsed valve (General Valve Series 9) into the source to cool the formed clusters. The generated cluster anions were mass-analyzed with the time-of-flight mass spectrometer. The cluster anions of interest were size-selected with a mass gate, decelerated by a momentum decelerator before crossing with the beam of another Nd:YAG laser (Continuum Surelite II-10, 266 nm) at the photodetachment region. The photoelectrons were energy-analyzed by using a magnetic-bottle photoelectron spectrometer. The photoelectron spectra were calibrated with the known spectra of Cu^- and Au^- ions taken under similar conditions. The resolution of the magnetic-bottle photoelectron spectrometer was about 40 meV at an electron kinetic energy of 1 eV.

2.2 Theoretical methods

The structural optimizations and frequency calculations were carried out using DFT with Becke's three-parameter and Lee–Yang–Parr's gradient-corrected correlation hybrid functional (B3LYP),[35,36] as implemented in the GAUSSIAN 09 program package.[37] The exchange–correlation potential and effective core pseudopotential LanL2DZ basis set[38] was used for the Nb atom, and Pople's all-electron 6-311+G(d) basis set was used for the Si atoms. No symmetry constraint was imposed during the full geometry optimizations. For all clusters, a large amount of initial structures reported in the literature were taken into account at all possible spin states. Additionally, we have used the swarm-intelligence based CALYPSO structure prediction software[39] for determining the global minima. Harmonic vibrational frequencies were calculated to confirm that the obtained structures were true minima on the potential energy surfaces. In order to obtain more accurate relative energies, the single-point energies of the $NbSi_n^{-/0}$ clusters were calculated by using the coupled-cluster methods including single and double, and perturbative triple excitation (CCSD(T))[40,41] with the aug-cc-pVDZ-PP basis set[42] used for the Nb atom and cc-pVDZ basis set[43] used for the Si atoms. Zero-point energy (ZPE) corrections were included for all the calculated energies.

3. Experimental results

The photoelectron spectra of $NbSi_n^-$ (n = 3–12) clusters recorded with 266 nm photons are presented in Fig. 1. The vertical detachment energies (VDEs) and the adiabatic detachment energies (ADEs) of the clusters obtained from their photoelectron spectra are summarized in Table 1. The VDEs of these clusters were estimated from the maxima of the first peaks, whereas the ADEs of these clusters were obtained by drawing a straight line along the leading edge of the first peaks to cross the baseline of spectra and then adding the instrumental resolution to the electron binding energy (EBE)

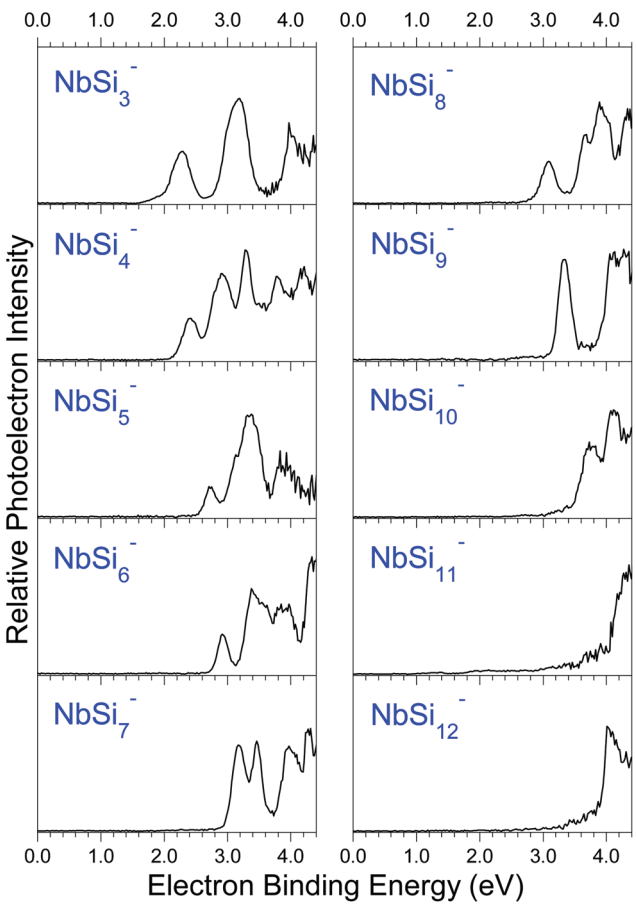

Fig. 1 Photoelectron spectra of $NbSi_n^-$ (n = 3–12) clusters recorded with 266 nm photons.

Table 1 Relative energies, theoretical VDEs and ADEs of the low-lying isomers of $NbSi_n^-$ (n = 3–12) clusters, as well as the experimental VDEs and ADEs estimated from their photoelectron spectra. The isomers labeled in bold are the most probable ones in the experiments

				VDE (eV)		ADE (eV)						VDE (eV)		ADE (eV)	
	Isomer	Sym	ΔE^a (eV)	Theo.[b]	Expt.[c]	Theo.[b]	Expt.[c]		Isomer	Sym	ΔE^a (eV)	Theo.[b]	Expt.[c]	Theo.[b]	Expt.[c]
$NbSi_3^-$	**3A**	C_{3v}	0.00	2.32	2.28	2.22	1.94	$NbSi_9^-$	**9A**	C_{3v}	0.00	3.23	3.32	3.05	3.14
	3B	C_{2v}	1.17	2.14		1.25			9B	C_1	0.34	3.01		2.92	
$NbSi_4^-$	**4A**	C_1	0.00	2.39	2.41	2.25	2.12		9C	C_1	0.48	3.21		3.13	
	4B	C_s	0.74	2.21		2.06			9D	C_1	0.64	3.68		3.44	
$NbSi_5^-$	**5A**	C_{4v}	0.00	2.74	2.74	2.71	2.50	$NbSi_{10}^-$	**10A**	C_1	0.00	3.61	3.73	3.40	3.41
	5B	C_1	0.46	2.69		2.56			10B	C_1	0.08	3.29		3.23	
	5C	C_s	0.92	2.28		2.21			10C	C_1	0.16	3.45		3.27	
	5D	C_s	0.97	2.47		2.34			10D	C_s	0.22	3.71		3.42	
$NbSi_6^-$	**6A**	C_s	0.00	2.91	2.92	2.84	2.72	$NbSi_{11}^-$	**11A**	C_{2v}	0.00	4.26	4.27	3.79	3.90
	6B	C_{3v}	0.21	3.01		2.64			11B	C_1	0.35	3.69		3.50	
	6C	C_2	0.57	2.99		2.64			11C	C_2	0.68	3.34		3.22	
	6D	C_s	0.61	2.83		2.53			11D	C_s	0.96	3.34		2.91	
$NbSi_7^-$	**7A**	C_s	0.00	3.07	3.19	2.94	2.99	$NbSi_{12}^-$	**12A**	D_{6h}	0.00	3.90	4.00	3.83	3.90
	7B	C_s	0.72	3.00		2.69			12B	C_1	1.05	3.46		3.29	
	7C	C_s	0.72	2.92		2.71			12C	C_1	1.07	3.95		3.63	
	7D	C_1	0.90	2.61		2.39			12D	C_1	1.25	3.43		3.19	
$NbSi_8^-$	**8A**	C_{2v}	0.00	3.01	3.08	2.84	2.79								
	8B	C_s	0.60	2.96		2.79									
	8C	C_s	0.62	2.74		2.54									
	8D	C_1	0.64	2.78		2.63									

[a] The ΔEs are calculated at the CCSD(T)/cc-PVDZ/Si/aug-cc-PVDZ-PP/Nb level of theory. [b] The ADEs and VDEs are calculated at the B3LYP/6-311+G(d)/Si/LanL2DZ/Nb level of theory. [c] The uncertainty of the experimental VDEs and ADEs is ±0.08 eV.

values at the crossing points. It is worth mentioning that the photoelectron spectra of $NbSi_n^-$ clusters with n = 6–12 had been measured previously with 213 nm photons in ref. 31. In this work, the low energy photons (266 nm) were used, therefore, we were able to observe better resolved spectral features.

As shown in Fig. 1, the spectrum of $NbSi_3^-$ reveals three peaks at 2.28, 3.17, and 3.97 eV. The spectrum of $NbSi_4^-$ has five peaks centered at 2.41, 2.92, 3.29, 3.80, and 4.18 eV, respectively. The spectrum of $NbSi_5^-$ shows a low intensity peak at 2.74 eV, followed by a shoulder peak at 3.13 eV, a high intensity broad peak at 3.35 eV, and some not well-separated peaks in the range of 3.7–4.3 eV. The spectrum of $NbSi_6^-$ presents a low intensity peak at 2.92 eV and five barely resolved peaks at 3.37, 3.58, 3.82, 3.98, and 4.33 eV, respectively. In the spectrum of $NbSi_7^-$, there are two overlapping strong peaks at 3.19 and 3.46 eV, followed by two additional high intensity peaks at 3.99 and 4.26 eV. For the spectrum of $NbSi_8^-$, there is a low intensity peak at 3.08 eV, followed by three barely resolved peaks at 3.67, 3.88, and 4.34 eV, respectively. The spectrum of $NbSi_9^-$ displays a high intensity sharp peak at 3.32 eV and two barely distinguished peaks at 4.09 and 4.29 eV. The spectrum of $NbSi_{10}^-$ has two major peaks at 3.73 and 4.10 eV. In the spectrum of $NbSi_{11}^-$, the onset of a broad peak at 4.27 eV can be observed. The spectrum of $NbSi_{12}^-$ shows a major peak at 4.00 eV.

4. Theoretical results

The typical low-lying isomers of $NbSi_n^-$ (n = 3–12) cluster anions are displayed in Fig. 2 with the most stable isomers on the left. The relative energies, theoretical VDEs and ADEs of these low-lying isomers are listed in Table 1, along with the experimental VDEs and ADEs for comparison. The bond lengths of the most stable isomers of $NbSi_n^{-/0}$ clusters are shown in Table 2. We also simulated the photoelectron spectra of the low-lying isomers based on theoretically generalized Koopman theorem (GKT).[44,45] For convenience, we call the simulated spectra as the density of states (DOS) spectra. The DOS spectra and experimental spectra are compared in Fig. 3. In the DOS spectra, the peak intensities are different from the experimental spectra because each transition is treated equally in the simulations. More information on the isomers can be found in the ESI.†

4.1 $NbSi_n^-$ (n = 3–12) anions

The most stable isomer of $NbSi_3^-$ (3A) is a C_{3v} symmetric pyramid structure with the Nb atom located at the C_3 axis. The calculated VDE (2.32 eV) of isomer 3A is in excellent agreement with the experimental value (2.28 eV) and its simulated DOS spectrum fits the peak positions and patterns of the experimental spectrum very well. The existence of isomer 3B can be ruled out because it is much higher in energy than isomer 3A by 1.17 eV. Therefore, we suggest isomer 3A to be the most probable structure detected in our experiments.

The lowest-lying isomer of $NbSi_4^-$ (4A) is a trigonal bipyramid structure with the Nb atom at the vertex. The calculated VDE (2.39 eV) of isomer 4A is in excellent agreement with the experimental value (2.41 eV) and its simulated DOS spectrum matches the peak positions and patterns of the experimental spectrum very well. Isomer 4B is much higher in energy than

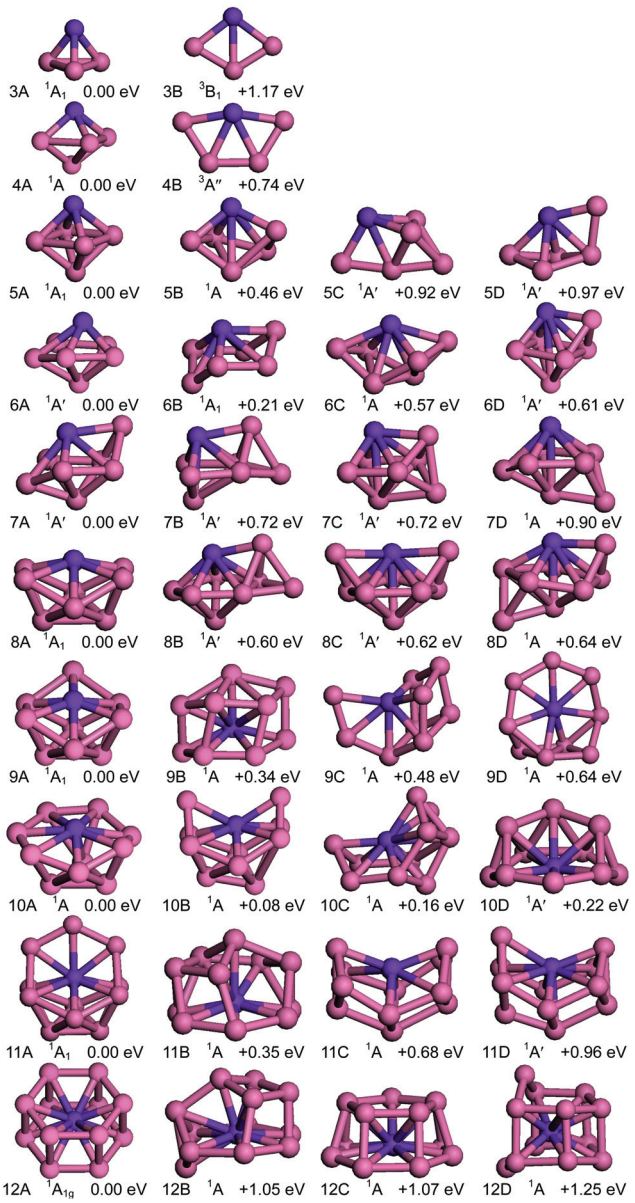

Fig. 2 Typical low-lying isomers of $NbSi_n^-$ (n = 3–12) anions. The relative energies are calculated at the CCSD(T)/cc-PVDZ/Si/aug-cc-PVDZ-PP/Nb level of theory. The pink and purple balls stand for the Si atoms and Nb atoms, respectively.

isomer 4A by 0.74 eV. Thus, we suggest that isomer 4A is the most probable structure observed in our experiments.

As for the $NbSi_5^-$ cluster, the most stable isomer (5A) is a C_{4v} symmetric tetragonal bipyramid structure with the Nb atom situated at the C_4 axis. The calculated VDE (2.74 eV) of isomer 5A is equal to the experimental value (2.74 eV) and its simulated DOS spectrum can reproduce the peak positions and patterns of the experimental spectrum. Isomers 5B, 5C, and 5D are higher in energy than isomer 5A by at least 0.46 eV. Thus, we suggest that isomer 5A is the most probable structure contributing to the photoelectron spectrum of $NbSi_5^-$.

Table 2 Bond lengths in the most stable isomers of $NbSi_n^{-/0}$ (n = 3–12) clusters

Isomer	Bond length (Å)	Isomer	Bond length (Å)
3A	Nb–Si = 2.37 Si–Si = 2.60	3A′	Nb–Si = 2.36–2.47 Si–Si = 2.46
4A	Nb–Si = 2.40–2.42 Si–Si = 2.38–2.71	4A′	Nb–Si = 2.46–2.64 Si–Si = 2.24
5A	Nb–Si = 2.48 Si–Si = 2.49–2.67	5A′	Nb–Si = 2.50 Si–Si = 2.48–2.64
6A	Nb–Si = 2.45–2.96 Si–Si = 2.35–2.81	6A′	Nb–Si = 2.45–3.07 Si–Si = 2.37–2.87
7A	Nb–Si = 2.49–2.77 Si–Si = 2.37–2.67	7A′	Nb–Si = 2.51–2.85 Si–Si = 2.33–2.76
8A	Nb–Si = 2.56–2.66 Si–Si = 2.48–2.74	8A′	Nb–Si = 2.56–2.70 Si–Si = 2.48–2.59
9A	Nb–Si = 2.52–2.65 Si–Si = 2.54–2.59	9A′	Nb–Si = 2.50–2.87 Si–Si = 2.45–2.85
10A	Nb–Si = 2.73–2.75 Si–Si = 2.33–2.84	10A′	Nb–Si = 2.36–3.11 Si–Si = 2.38–3.21
11A	Nb–Si = 2.63–2.68 Si–Si = 2.36–2.61	11A′	Nb–Si = 2.70–3.54 Si–Si (h) = 2.41–3.54 Si–Si (v) = 2.37–3.54
12A	Nb–Si = 2.71 Si–Si (h) = 2.42 Si–Si (v) = 2.45	12A′	Nb–Si = 2.71 Si–Si (h) = 2.43 Si–Si (v) = 2.41

(h): horizontal, (v): vertical.

With respect to the $NbSi_6^-$ cluster, the most stable isomer (6A) is a distorted pentagonal bipyramid structure with the Nb atom at the vertex. The calculated VDE (2.91 eV) of isomer 6A is in excellent agreement with the experimental value (2.92 eV) and its simulated DOS spectrum is in reasonable agreement with the experimental spectrum. Isomers 6B, 6C and 6D are higher in energy than isomer 6A by at least 0.21 eV. Therefore, we suggest isomer 6A to be the most probable one contributing to the photoelectron spectrum of $NbSi_6^-$.

With regard to the $NbSi_7^-$ cluster, the lowest-lying isomer (7A) can be built by an additional Si atom face-capping the right side of the distorted pentagonal bipyramid of $NbSi_6^-$ (6A). The calculated VDE (3.07 eV) of isomer 7A is in good agreement with the experimental value (3.19 eV) and its simulated DOS spectrum resembles the experimental spectrum. Isomers 7B, 7C, and 7D are higher in energy than isomer 7A by at least 0.72 eV. Therefore, we suggest that isomer 7A is the most probable structure detected in our experiments.

The lowest-lying isomer of $NbSi_8^-$ (8A) is a C_{2v} symmetric boat-shaped structure with the Nb atom located at the C_2 axis. The calculated VDE (3.01 eV) of isomer 8A is in good agreement with the experimental value (3.08 eV) and its simulated DOS spectrum fits the peak positions and patterns of the experimental spectrum very well. Isomers 8B, 8C, and 8D are higher in energy than isomer 8A by at least 0.60 eV. Thus, we suggest that isomer 8A is the most probable structure observed in our experiments.

The global minimum structure of $NbSi_9^-$, isomer 9A, can be constructed by adding an additional Si atom to face-cap the boat-shaped structure of $NbSi_8^-$. The calculated VDE (3.23 eV) of isomer 9A is in good agreement with the experimental value (3.32 eV) and its simulated DOS spectrum fits the peak

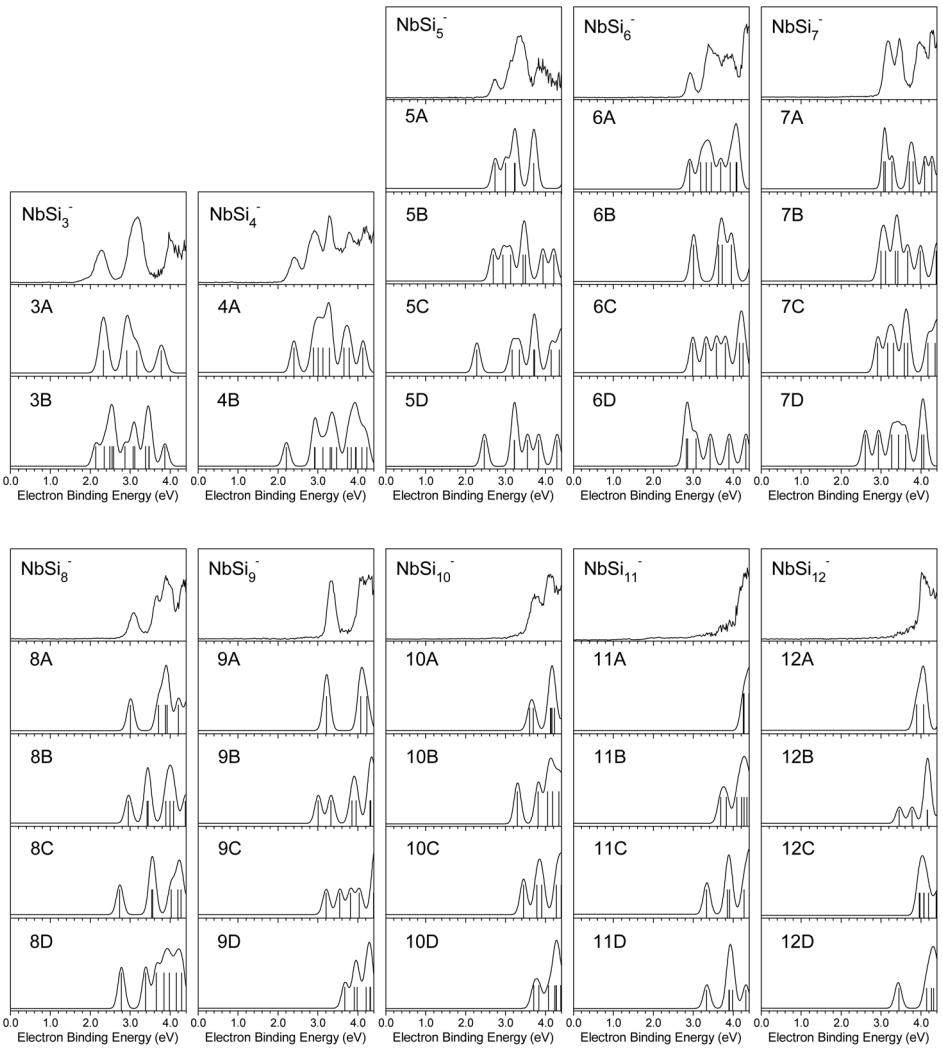

Fig. 3 Comparison between the experimental photoelectron spectra and simulated DOS spectra of the low-lying isomers of $NbSi_n^-$ (n = 3–12) clusters. The simulated spectra were obtained by fitting the distribution of the transition lines with unit area Gaussian functions of 0.20 eV full width at half maximum.

positions and patterns of the experimental spectrum very well. Isomers 9B, 9C, and 9D are higher in energy than isomer 9A by at least 0.34 eV. Therefore, we suggest isomer 9A to be the most probable structure observed in our experiments.

The most stable isomer of $NbSi_{10}^-$ (10A) can be constructed by adding two additional Si atoms to face-cap one side of the boat-shaped structure of $NbSi_8^-$ (8A). The calculated VDE (3.61 eV) of isomer 10A is in good agreement with the experimental value (3.73 eV) and its simulated DOS spectrum is in reasonable agreement with the experimental spectrum. Although isomer 10B is higher in energy than isomer 10A by only 0.08 eV, its calculated VDE (3.29 eV) is much lower than the experimental value and its simulated DOS spectrum is different from the experimental spectrum. Isomers 10C and 10D are higher in energy than isomer 10A by 0.16 and 0.22 eV, respectively. Therefore, we suggest that isomer 10A is the most probable structure detected in our experiments.

The lowest-lying isomer of $NbSi_{11}^-$ (11A) can be described as a C_{2v} symmetric basket-shaped endohedral structure with three Si atoms forming the handle of the basket, the remaining Si atoms forming the containing part of the basket, and the Nb atom being encapsulated into the basket. It can also be viewed as adding three Si atoms to face-cap on the top of the boat-shaped structure of $NbSi_8^-$ with two Si atoms interacting with the two ends of the boat, respectively, and the third Si atom bridging the two Si atoms. The calculated VDE (4.26 eV) of isomer 11A is in excellent agreement with the experimental value (4.27 eV), and its simulated DOS spectrum can reproduce the peak positions and patterns of the experimental spectrum. Isomers 11B, 11C, and 11D are higher in energy than isomer 11A by at least 0.35 eV. Therefore, isomer 11A is regarded as the most probable one observed in our experiments.

The most stable isomer of $NbSi_{12}^-$ (12A) is found to be a D_{6h} symmetric hexagonal prism with the Nb atom at the center. The calculated VDE (3.90 eV) of isomer 12A is in good

agreement with the experimental value (4.00 eV) and its simulated DOS spectrum fits the peak positions and patterns of the experimental spectrum very well. Isomers 12B, 12C, and 12D are much higher in energy than isomer 12A by at least 1.05 eV. Therefore, isomer 12A is considered as the most probable structure detected in our experiments.

4.2 Neutral $NbSi_n$ (n = 3–12)

We have also optimized the structures of neutral $NbSi_n$ (n = 3–12) clusters with DFT calculations at the B3LYP/6-311+G(d)/Si/LanL2DZ/Nb level of theory. The typical low-lying isomers and their relative energies (ΔEs) calculated at the CCSD(T)/cc-PVDZ/Si/aug-cc-PVDZ-PP/Nb level of theory are displayed in Fig. 4. The most stable structures of neutral $NbSi_n$ clusters are similar to those of $NbSi_n^-$ anions with slight differences in the bond lengths, except that the structures of $NbSi_4$, $NbSi_{10}$, and $NbSi_{11}$ are different from their anionic counterparts. For $NbSi_4$, the most stable isomer (4A′) is a fan-shaped structure with the Nb atom at its circle center, which is similar to isomer 4B of $NbSi_4^-$. The lowest-lying isomer (10A′) of $NbSi_{10}$ can be regarded as two additional Si atoms capping the two terminal Si–Si bonds of the boat-shaped structure of $NbSi_8$ (8A′), respectively, which is analogous to isomer 10B of $NbSi_{10}^-$. As for $NbSi_{11}$, the most stable isomer (11A′) is an exohedral structure and can be viewed as adding a Si_5 five-membered ring to face-cap the top of the distorted pentagonal bipyramid of $NbSi_6$ (6A′). The previous DFT calculations predicted the most stable isomer of $NbSi_{10}$ to be an endohedral bicapped tetragonal antiprism.[25] In this work, we have determined the bicapped tetragonal antiprism structure of $NbSi_{10}$, but found that it is much higher in energy than the exohedral structure (10A′) by 2.02 eV, at the CCSD(T) level of theory.

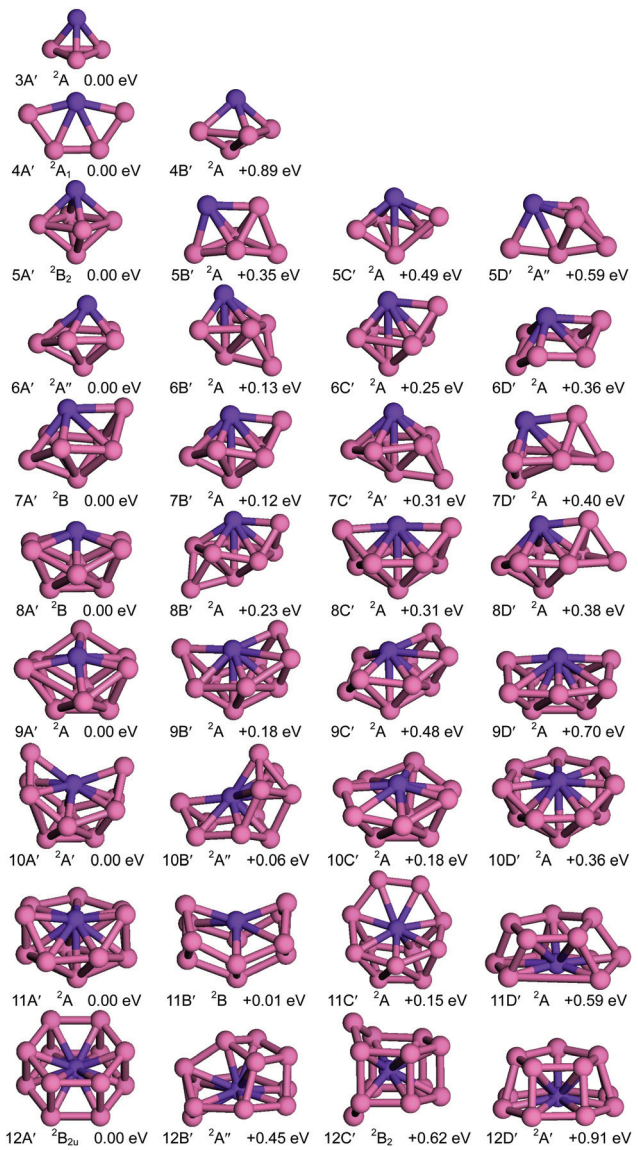

Fig. 4 Typical low-lying isomers of neutral $NbSi_n$ (n = 3–12). The relative energies are calculated at the CCSD(T)/cc-PVDZ/Si/aug-cc-PVDZ-PP/Nb level of theory. The pink and purple balls stand for the Si atoms and Nb atoms, respectively.

5. Discussion

Fig. 5 shows the change of experimental and theoretical VDEs of the most stable isomers *versus* the number of Si atoms. It can be seen that the calculated VDEs are in excellent agreement with the experimental VDEs with average derivations of ~0.09 eV, confirming that the theoretical methods used in this work are reliable. It is found that the Nb atom in $NbSi_n^{-/0}$ prefers to occupy the high coordination sites to form more Nb–Si bonds. For both anionic and neutral $NbSi_n^{-/0}$ clusters with n = 3–7, the dominant geometries are all exohedral structures with the Nb atom face-capping the Si_n frameworks. The boat-shaped structures appear at n = 8 for both anionic and neutral clusters and the openings of the boat-shaped structures remain unclosed in $NbSi_{9-10}^{-/0}$ clusters. The $NbSi_{11}^-$ anion is an endohedral structure, whereas the neutral $NbSi_{11}$ is an exohedral structure. At n = 12, both the $NbSi_{12}^-$ anion

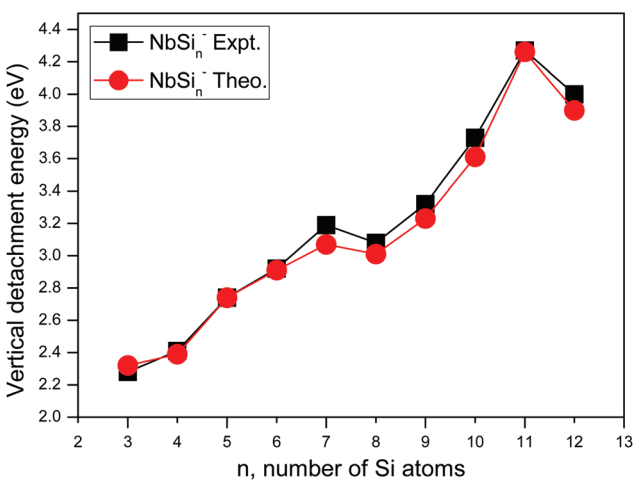

Fig. 5 Experimental and theoretical VDEs of $NbSi_n^-$ (n = 3–12) clusters *versus* n, the number of Si atoms.

and neutral $NbSi_{12}$ are D_{6h} symmetric perfect hexagonal prisms with the Nb atom at the center, which is consistent with the previous theoretical results.[24,25,27] As shown in Table 2, the height (Si–Si (v)) of the hexagonal prism structure of neutral $NbSi_{12}$ (12A′) is shortened by 0.04 Å, while the sides (Si–Si (h)) of the hexagonal prism structure of neutral $NbSi_{12}$ are lengthened by 0.01 Å, relative to those of the $NbSi_{12}^-$ anion (12A). It appears that the changes of the $NbSi_n^-$ photoelectron spectra are related to their structural evolution. The spectral profiles of $NbSi_{3-7}^-$ are rather similar to each other except that their VDEs increase gradually with the number of Si atoms, which may be attributed to their similar structures. Whereas the change of the spectral profile at n = 8 may be associated with the formation of a boat-shaped structure. The structures of $NbSi_{9-11}^-$ are derived from the boat-shaped structure of $NbSi_8^-$, which perhaps gives them similar spectral profiles except that their VDEs increase gradually with the number of Si atoms. The structure of $NbSi_{12}^-$ is not simply evolved from the boat-shaped structure of $NbSi_8^-$ due to the formation of more symmetric geometry, which may explain why the spectral profile of $NbSi_{12}^-$ is different from that of $NbSi_8^-$. The most stable geometric structures of $NbSi_6^-$, $NbSi_{9-11}^-$, $NbSi_4$, and $NbSi_{8-11}$ determined in this work are different from those in ref. 27, probably because the reference used the B3LYP functional for single-point energy calculations, while we used the CCSD(T) method to calculate the single-point energies.

It is worth mentioning that the structural evolution of the anionic and neutral $NbSi_n$ clusters is somewhat different from their cations. Regarding the $NbSi_n^+$ cations, the water adsorption reactivity experiments suggested that $NbSi_{13}^+$ is the threshold size of the endohedral structures rather than $NbSi_{12}^+$.[32] The far-infrared spectrum of $NbSi_{12}^+$ measured *via* infrared multi-photon dissociation (IR-MPD) experiments also suggested the most stable structure of $NbSi_{12}^+$ to be exohedral.[33] We have also optimized the structures of the $NbSi_{12}^+$ cation and calculated the relative energies of the stable isomers, and found that the most stable structure of the $NbSi_{12}^+$ cation is exohedral, which is very similar to the most stable structure reported in ref. 33. The endohedral hexagonal prism of the $NbSi_{12}^+$ cation is higher in energy than the exohedral structure by 0.30 eV at the CCSD(T) level of theory (and by 0.11 eV at the B3LYP level of theory). The different structural evolution of the cationic $NbSi_n^+$ clusters is more likely induced by the removal of the electrons, which has also been found in the case of $VSi_n^{+/0/-}$ clusters.[32]

It would be interesting to compare the structures of the $NbSi_n^-$ clusters with those of the VSi_n^- clusters. The structures of VSi_n^- (n = 2–6) have been reported by Xu *et al.*,[34] those of VSi_n^- (n = 7–11) by Deng *et al.*,[46] and that of VSi_{12}^- by Huang *et al.*[8] At n = 2–7, the photoelectron spectra of $NbSi_n^-$ are rather similar to those of VSi_n^- except that the VDEs of $NbSi_n^-$ are slightly higher than those of VSi_n^-. The most stable geometric structures of $NbSi_n^-$ and VSi_n^- are all exohedral structures with the metals face-capping the Si_n frameworks and occupying the high coordination sites. Their similar geometric structures may explain why $NbSi_n^-$ and VSi_n^- have similar spectral features. At n = 8–10, the spectral profiles of $NbSi_{8-10}^-$ are different from those of VSi_{8-10}^-. Comparing the most stable structures of $NbSi_n^-$ with those of VSi_n^-, we found that $NbSi_{8-10}^-$ can still be viewed as exohedral structures because the Nb atom slightly protrudes out from the boat-shaped framework, probably because the atomic radius of the Nb atom is larger than that of the V atom. This implies that the changes in the photoelectron spectra of $NbSi_n^-$ and VSi_n^- are related to their structural evolution. At n = 11, the spectral feature of $NbSi_{11}^-$ is very similar to that of VSi_{11}^-, but the experimental VDE of $NbSi_{11}^-$ is higher in energy than that of VSi_{11}^- by 0.21 eV. The ground state isomers of both $NbSi_{11}^-$ and VSi_{11}^- are basket-shaped endohedral structures, more likely lead to $NbSi_{11}^-$ and VSi_{11}^- having similar spectral features. At n = 12, the experimental VDE of $NbSi_{12}^-$ is higher in energy than that of VSi_{12}^- by 0.18 eV. Only one spectral feature of $NbSi_{12}^-$ is observed in the experimental spectrum due to its high VDE. The global minima of both $NbSi_{12}^-$ and VSi_{12}^- are perfect D_{6h} symmetric hexagonal prisms with a metal atom at the center. However, the height and sides (2.45 and 2.42 Å) of the $NbSi_{12}^-$ hexagonal prism are slightly longer than those (2.39 and 2.36 Å) of VSi_{12}^-, which may also be attributed to the larger atomic radius of the Nb atom than that of the V atom.

To further investigate the chemical bonding properties of $NbSi_{12}^-$, we analyzed the molecular orbital diagrams of the most stable isomer (12A, $^1A_{1g}$) and displayed them in Fig. 6.

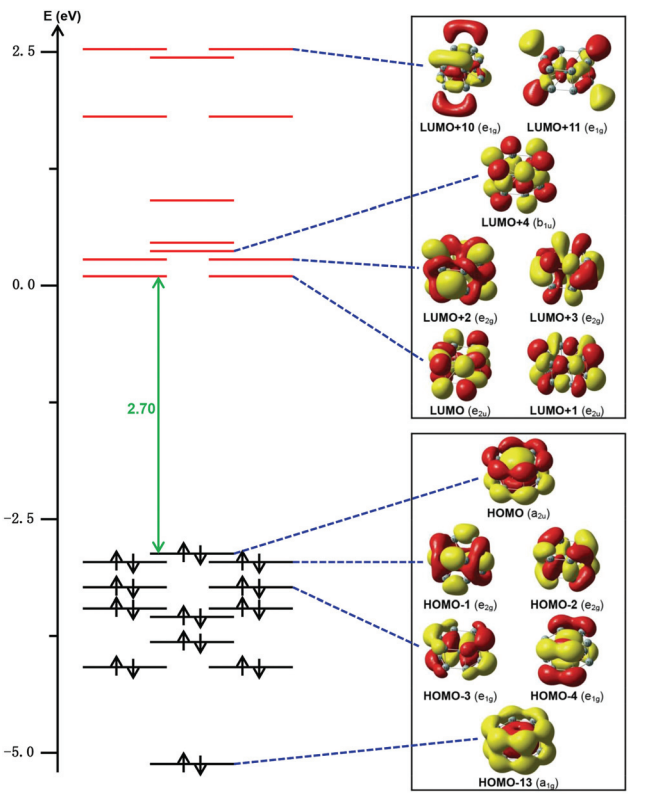

Fig. 6 Molecular orbitals of the D_{6h} symmetric hexagonal prism of the $NbSi_{12}^-$ anion (isosurface value = 0.018). These orbitals in the same row are energetically degenerate orbitals.

The HOMOs are all doubly occupied and the LUMO is higher in energy than the HOMO by 2.70 eV, indicating that the $NbSi_{12}^-$ anion has a shell-closed electronic structure with a large HOMO–LUMO gap. It is worth mentioning that the previous calculations found that the HOMO–LUMO gaps calculated with the BP86 functional are lower than those with the B3LYP functional.[29,47] To confirm this, we calculated the HOMO–LUMO gap of $NbSi_{12}^-$ using the BP86 functional and found that it gives a HOMO–LUMO gap of 1.80 eV, smaller than that from the B3LYP functional by 0.90 eV. The HOMO has an interesting sandwich shape with the electron cloud delocalized in the planes of a pair of six-membered Si_6 rings, more likely due to the interactions between the $5p_z$ orbital of the Nb atom and the 3s3p hybridized orbitals of the Si_{12} cage. The $5p_z$ orbital of the Nb atom has 13.89% contribution to the HOMO, while the 3s3p hybridized orbitals of 12 Si atoms have 86.11% contribution to the HOMO. The HOMO–1 and HOMO–2 are two energetically degenerate orbitals, and each has 12.61% contribution from the $4d_{xy}$ and $4d_{x^2-y^2}$ orbitals of the Nb atom and 87.39% contribution from the 3s3p hybridized orbitals of the Si atoms. The $4d_{xz}$ and $4d_{yz}$ orbitals of the Nb atom and the 3s3p hybridized orbitals of the Si atoms are mainly included in the HOMO–3 and HOMO–4, which are two energetically degenerate orbitals and each has 47.83% contribution from the Nb atom and 52.17% contribution from the 12 Si atoms. The $4d_{z^2}$ orbital of the Nb atom and the 3s3p hybridized orbitals of the Si atoms are mainly involved in the HOMO–13, which has 4.74% contribution from the Nb atom and 95.26% contribution from the 12 Si atoms. The LUMO and LUMO–1 have no contribution from the 4d orbitals of the Nb atom and the 3s3p hybridized orbitals of the 12 Si atoms. The five 4d orbital compositions of the Nb atom and the 3s3p hybridized orbitals of the Si atoms can also be found in the LUMO+2, LUMO+3, LUMO+4, LUMO+10, and LUMO+11. This suggests that the Nb 4d – Si 3s/3p antibonding character drifts up into the vacant orbitals, and the 4d orbitals of the Nb atom in the HOMOs are involved in bonding rather than antibonding. These molecular orbitals suggest that there are interactions between the 4d orbitals of the Nb atom and the 3s3p hybridized orbitals of the Si_{12} cage, which is similar to the interactions between the 5d orbitals of the Au atom and the 4s4p hybridized orbitals of the Ge_{12} cage.[48] The valence electrons are delocalized over the whole $NbSi_{12}^-$ with most of them surrounding around the Nb atom. The delocalized Nb–Si_{12} ligand interactions may contribute to the stability of the D_{6h} symmetric hexagonal prism. In addition, the perfect D_{6h} symmetric hexagonal prism of $NbSi_{12}^-$ would be electronically stable according to the 18-electron rule,[8,49–57] because each Si atom interacts with three neighboring Si atoms and the central Nb atom, thus, each Si atom can donate one valence electron to the Nb atom considering electron-precise bonding, with five valence electrons of the Nb atom and the addition of the excess electron, the total number of effective valence electrons on the Nb atom adds up to 18 electrons.

We also analyzed the bonding properties of $NbSi_{12}^-$ using the adaptive natural density partitioning (AdNDP) method developed by Zubarev and Boldyrev.[58] The total number of valence electrons in the $NbSi_{12}^-$ anion (12A, $^1A_{1g}$) is 54, which includes 5 valence electrons of the Nb atom, 48 valence electrons of the 12 Si atoms, and an excess electron. As shown in Fig. 7, we can approximately extract eighteen 2c–2e Si–Si bonds including 36 valence electrons of the $NbSi_{12}^-$ anion. The remaining 18 valence electrons are distributed throughout the additional 9 delocalized $NbSi_n$ MOs. The 9 delocalized MOs include four 4c–2e $NbSi_3$ bonds (electronic occupation is equal to 1.81 |e|), two 5c–2e $NbSi_4$ bonds (electronic occupation is equal to 1.94 |e|), two 7c–2e $NbSi_6$ bonds (electronic occupation is equal to 1.94 |e|), and one 13c–2e $NbSi_{12}$ bond (electronic occupation is equal to 2.00 |e|). We found that the Si–Si interactions are mainly σ bonds, while the Nb–Si interactions are prominently dominated by π bonds. This indicates that the delocalized Nb–Si interactions and Si–Si interactions are important for the structural stability of the D_{6h} symmetric hexagonal prism of the $NbSi_{12}^-$ anion.

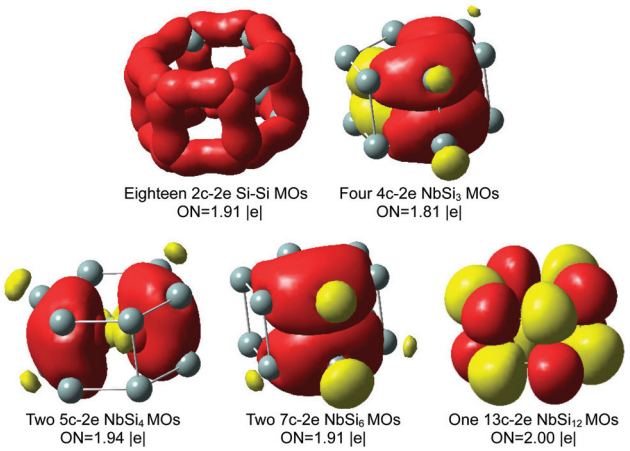

Fig. 7 Adaptive natural density partitioning (AdNDP) molecular orbitals (contour values $\psi = \pm 0.038$ au) of D_{6h} symmetric hexagonal prism of the $NbSi_{12}^-$ anion (12A, $^1A_{1g}$) are obtained by using the B3LYP/AVTZ-PP//AVTZ method. (ON = electronic occupation).

6. Conclusions

We measured the photoelectron spectra of $NbSi_n^-$ (n = 3–12) anions and investigated the structures of $NbSi_n^{-/0}$ (n = 3–12) clusters with *ab initio* calculations. We found that the Nb atom in $NbSi_n^{-/0}$ prefers to occupy the high coordination sites to form more Nb–Si bonds. For both anionic and neutral $NbSi_n$ clusters with n = 3–7, the dominant geometries are all exohedral structures with the Nb atom face-capping the Si_n frameworks. The boat-shaped structures appear at n = 8 for both anionic and neutral clusters and the openings of the boat-shaped structures are still unclosed in the $NbSi_{9-10}^{-/0}$ clusters. The most stable structure of the $NbSi_{11}^-$ anion is endohedral, whereas that of neutral $NbSi_{11}$ is exohedral. At n = 12, the global minima of both the $NbSi_{12}^-$ anion and neutral $NbSi_{12}$ are D_{6h} symmetric hexagonal prisms with the Nb atom at the

center. The D_{6h} symmetric hexagonal prism of the $NbSi_{12}^-$ anion is electronically stable as it obeys the 18-electron rule and has a shell-closed electronic structure with a large HOMO–LUMO gap of 2.70 eV. The molecular orbital analysis of $NbSi_{12}^-$ suggests that there are interactions between the 4d orbitals of the Nb atom and the 3s3p hybridized orbitals of the Si_{12} cage, and the delocalized Nb–Si_{12} ligand interactions may make the D_{6h} symmetric hexagonal prism of $NbSi_{12}^-$ stable. The AdNDP analysis shows that the Si–Si interactions are mainly σ bonds, while the Nb–Si interactions are prominently dominated by π bonds, which are important for the structural stability of the D_{6h} symmetric hexagonal prism.

Acknowledgements

This work was supported by the National Natural Science Foundation of China (Grant No. 21103202, 21273246, and 21303214) and the Chinese Academy of Sciences (Grant No. QYZDB-SSW-SLH024). The theoretical calculations are conducted on the China Scientific Computing Grid (ScGrid) of the Supercomputing Center, Computer Network Information Center of the Chinese Academy of Sciences.

References

1 S. M. Beck, *J. Chem. Phys.*, 1987, **87**, 4233–4234.
2 F. Hagelberg, C. Xiao and W. A. Lester, *Phys. Rev. B: Condens. Matter*, 2003, **67**, 035426.
3 N. Uchida, T. Miyazaki and T. Kanayama, *Phys. Rev. B: Condens. Matter*, 2006, **74**, 205427.
4 H. G. Xu, X. Y. Kong, X. J. Deng, Z. G. Zhang and W. J. Zheng, *J. Chem. Phys.*, 2014, **140**, 024308.
5 T. Iwasa and A. Nakajima, *J. Phys. Chem. C*, 2012, **116**, 14071–14077.
6 V. Kumar and Y. Kawazoe, *Phys. Rev. Lett.*, 2001, **87**, 045503.
7 A. K. Singh, T. M. Briere, V. Kumar and Y. Kawazoe, *Phys. Rev. Lett.*, 2003, **91**, 146802.
8 X. M. Huang, H. G. Xu, S. J. Lu, Y. Su, R. B. King, J. J. Zhao and W. J. Zheng, *Nanoscale*, 2014, **6**, 14617–14621.
9 X. M. Huang, S. J. Lu, X. Q. Liang, Y. Su, L. W. Sai, Z. G. Zhang, J. J. Zhao, H. G. Xu and W. J. Zheng, *J. Phys. Chem. C*, 2015, **119**, 10987–10994.
10 J. G. He, K. C. Wu, R. J. Sa, Q. H. Li and Y. Q. Wei, *Chem. Phys. Lett.*, 2010, **490**, 132–137.
11 C. L. Reis, J. L. Martins and J. M. Pacheco, *Phys. Rev. B: Condens. Matter*, 2007, **76**, 233406.
12 C. Berkdemir and O. Gülseren, *Phys. Rev. B: Condens. Matter*, 2009, **80**, 115334.
13 S. A. Claridge, A. W. Castleman, S. N. Khanna, C. B. Murray, A. Sen and P. S. Weiss, *ACS Nano*, 2009, **3**, 244–255.
14 A. N. Andriotis, G. Mpourmpakis, G. E. Froudakis and M. Menon, *New J. Phys.*, 2002, **4**, 78.
15 Z. F. Liu, X. Q. Wang, J. T. Cai and H. J. Zhu, *J. Phys. Chem. C*, 2015, **119**, 1517–1523.
16 H. Aubin, C. A. Marrache-Kikuchi, A. Pourret, K. Behnia, L. Bergé, L. Dumoulin and J. Lesueur, *Phys. Rev. B: Condens. Matter*, 2006, **73**, 094521.
17 D. Olaya, P. D. Dresselhaus and S. P. Benz, *IEICE Trans. Electron*, 2010, **E93-C**, 463–467.
18 S. Lefranc, M. Piat, J. P. Torre, E. Bréelle, B. Leriche, L. Dumoulin, L. Bergé, C. Evesque and F. Pajot, *Nucl. Instrum. Methods Phys. Res., Sect. A*, 2006, **559**, 468–470.
19 C. A. Marrache-Kikuchi, L. Berge, S. Collin, C. Dobrea, L. Dumoulin, A. Juillard and S. Marnieros, *Nucl. Instrum. Methods Phys. Res., Sect. A*, 2006, **559**, 579–581.
20 S. Marnieros, L. Berge, A. Broniatowski, M. Chapellier, S. Collin, O. Crauste, X. Defay, Y. Dolgorouky, L. Dumoulin, A. Juillard, *et al.*, *J. Low Temp. Phys.*, 2008, **151**, 835–840.
21 B. P. Bewlay, M. R. Jackson and H. A. Lipsitt, *Metall. Mater. Trans. A*, 1996, **27**, 3801.
22 O. Crauste, C. A. Marrache-Kikuchi, L. Bergé, D. Stanescu and L. Dumoulin, *J. Phys.: Conf. Ser.*, 2009, **150**, 042019.
23 T. Proslier, J. A. Klug, J. W. Elam, H. Claus, N. G. Becker and M. J. Pellin, *J. Phys. Chem. C*, 2011, **115**, 9477–9485.
24 P. Sen and L. Mitas, *Phys. Rev. B: Condens. Matter*, 2003, **68**, 155404.
25 G. K. Gueorguiev, J. M. Pacheco, S. Stafström and L. Hultman, *Thin Solid Films*, 2006, **515**, 1192–1196.
26 J. Pacheco, G. Gueorguiev and J. Martins, *Phys. Rev. B: Condens. Matter*, 2002, **66**, 033401.
27 X. X. Xia, A. Hermann, X. Y. Kuang, Y. Y. Jin, C. Lu and X. D. Xing, *J. Phys. Chem. C*, 2016, **120**, 677–684.
28 X. J. Li, Q. Han, X. H. Yang, R. J. Song and L. M. Song, *Chem. Phys. Lett.*, 2016, **659**, 93–99.
29 X. J. Li, Z. J. Yan and S. N. Li, *J. Comput. Chem.*, 2016, **37**, 2316–2323.
30 K. D. Gunaratne, C. Berkdemir, C. L. Harmon and A. W. Castleman, *Phys. Chem. Chem. Phys.*, 2013, **15**, 6068–6079.
31 K. Koyasu, J. Atobe, S. Furuse and A. Nakajima, *J. Chem. Phys.*, 2008, **129**, 214301.
32 K. Koyasu, J. Atobe, M. Akutsu, M. Mitsui and A. Nakajima, *J. Phys. Chem. A*, 2007, **111**, 42–49.
33 X. J. Li, P. Claes, M. Haertelt, P. Lievens, E. Janssens and A. Fielicke, *Phys. Chem. Chem. Phys.*, 2016, **18**, 6291–6300.
34 H. G. Xu, Z. G. Zhang, Y. Feng, J. Y. Yuan, Y. C. Zhao and W. J. Zheng, *Chem. Phys. Lett.*, 2010, **487**, 204–208.
35 C. Lee, W. Yang and R. G. Parr, *Phys. Rev. B: Condens. Matter*, 1988, **37**, 785–789.
36 A. D. Becke, *J. Chem. Phys.*, 1993, **98**, 5648–5652.
37 M. J. Frisch, G. W. Trucks, H. B. Schlegel, G. E. Scuseria, M. A. Robb, J. R. Cheeseman, G. Scalmani, V. Barone, B. Mennucci and K. A. Peterson, *et al.*, *Gaussian 09, Revision A.02*, Gaussian, Inc., Wallingford, CT, 2009.
38 P. J. Hay and W. R. Wadt, *J. Chem. Phys.*, 1985, **82**, 270–283.
39 J. Lv, Y. C. Wang, L. Zhu and Y. M. Ma, *J. Chem. Phys.*, 2012, **137**, 084104.
40 G. D. Purvis and R. J. Bartlett, *J. Chem. Phys.*, 1982, **76**, 1910–1918.
41 G. E. Scuseria and H. F. Schaefer, *J. Chem. Phys.*, 1989, **90**, 3700–3703.

42 K. A. Peterson, D. Figgen, M. Dolg and H. Stoll, *J. Chem. Phys.*, 2007, **126**, 124101.
43 D. E. Woon and T. H. Dunning, *J. Chem. Phys.*, 1993, **98**, 1358–1371.
44 D. J. Tozer and N. C. Handy, *J. Chem. Phys.*, 1998, **109**, 10180–10189.
45 J. Akola, M. Manninen, H. H. kkinen, U. Landman, X. Li and L. S. Wang, *Phys. Rev. B: Condens. Matter*, 1999, **60**, 297–300.
46 X. J. Deng, X. Y. Kong, H. G. Xu, X. L. Xu, G. Feng and W. J. Zheng, *J. Phys. Chem. C*, 2015, **119**, 11048–11055.
47 V. T. Ngan, P. Gruene, P. Claes, E. Janssens, A. Fielicke, M. T. Nguyen and P. Lievens, *J. Am. Chem. Soc.*, 2010, **132**, 15589–15602.
48 S. J. Lu, L. R. Hu, X. L. Xu, H. G. Xu, H. Chen and W. J. Zheng, *Phys. Chem. Chem. Phys.*, 2016, **18**, 20321–20329.
49 W. D. Knight, K. Clemenger, W. A. de Heer, W. A. Saunders, M. Y. Chou and M. L. Cohen, *Phys. Rev. Lett.*, 1984, **52**, 2141–2143.
50 P. Pyykkö, *J. Organomet. Chem.*, 2006, **691**, 4336–4340.
51 J. A. W. Castleman and S. N. Khanna, *J. Phys. Chem. C*, 2009, **113**, 2664–2675.
52 V. M. Medel, A. C. Reber, V. Chauhan, P. Sen, A. M. Koster, P. Calaminici and S. N. Khanna, *J. Am. Chem. Soc.*, 2014, **136**, 8229–8236.
53 H. Hiura, T. Miyazaki and T. Kanayama, *Phys. Rev. Lett.*, 2001, **86**, 1733–1736.
54 R. Pandey, B. K. Rao, P. Jena and M. A. Blanco, *J. Am. Chem. Soc.*, 2001, **123**, 3799–3808.
55 K. Miyajima, A. Nakajima, S. Yabushita, M. B. Knickelbein and K. Kaya, *J. Am. Chem. Soc.*, 2004, **126**, 13202–13203.
56 T. D. Jaeger, D. Heijnsbergen, S. J. Klippenstein, G. Helden, G. Meijer and M. A. Duncan, *J. Am. Chem. Soc.*, 2004, **126**, 10981–10991.
57 K. Miyajima, S. Yabushita, M. B. Knickelbein and A. Nakajima, *J. Am. Chem. Soc.*, 2007, **129**, 8473–8480.
58 D. Y. Zubarev and A. I. Boldyrev, *Phys. Chem. Chem. Phys.*, 2008, **10**, 5207–5217.